J. Fluid Mech. (1979), *vol.* 94, *part* 2, *pp.* 353–367
Printed in Great Britain

On the formation of bubbles in gas-particulate fluidized beds

By JEROME B. FANUCCI, NATHAN NESS AND RUEY-HOR YEN

Department of Aerospace Engineering, West Virginia University, Morgantown, West Virginia 26506

(Received 2 October 1978 and in revised form 3 January 1979)

The method of characteristics is applied to the nonlinear equations describing two-phase flow in a fluidized bed. The method shows how a small disturbance changes with time and distance and can, eventually, produce a flow discontinuity similar to a shock wave in gases. The parameters entering the analysis are the amplitude of the initial disturbance, the wavelength of the original disturbance, the particulate pressure function, the particulate size, the uniform fluidization voidage, the uniform fluidization velocity, the fluid viscosity, the particulate density, and the fluid density. A parametric study shows that the following factors delay shock formation: a decrease in particulate size, an increase in bed density, an increase in fluid viscosity, and a decrease in particulate density. Experimental data on bubble formation in gas-particulate fluidized beds show that these same factors delay bubble formation. It is concluded, therefore, that the shock front and the bubble front are one and the same thing.

1. Introduction

A satisfactory explanation for the origin of bubbles in fluidized beds appears non-existent. El-Kaissy & Homsy (1976) in their recent review of the problem note this by stating: 'Thus to date, the origin of bubbles has been unexplained.'

Several investigators (e.g. Jackson 1963, part I; Pigford & Baron 1965; Garg & Pritchett 1975) have considered the formation of bubbles to be related to an instability in the state of uniform fluidization. They have shown that a small disturbance imposed on the uniformly fluidized bed can grow with time. However, their analyses are restricted to linearized stability theory and as noted by Jackson (1963, part II): 'The fact that small disturbances begin to grow is, however, no guarantee that the growth will continue to develop into true voids, or bubbles. Once their amplitude becomes finite, the nonlinearities in the equations of motion can no longer be neglected...' Thus, as stated by Jackson, and as demonstrated in the present paper, linear stability theory is not the proper mechanism to exhibit bubble formation.

Another approach is that proposed by Ruckenstein & Tzeculescu–Filipescu (1967) who assumed that a dense homogeneously fluidized system can pass into a heterogenous system when a certain critical condition is reached. Such a critical condition was given by Wallis (1962), who stated that bubbles are shock waves which arise when the rising velocity of the continuity waves exceeds the propagation velocity of the dynamic waves. This idea was investigated in papers by Verloop & Heertjes (1970), Verloop & Heertjes (1974), and Verloop, Heertjes & Lerk (1974). However, in the

0022-1120/79/4285-7370 $02.00

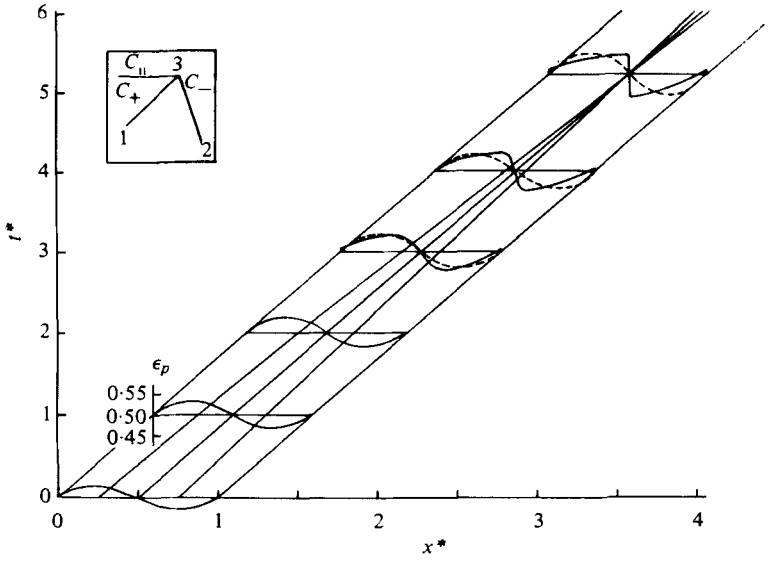

FIGURE 1. Propagation of the particulate voidage ϵ_p. ----, linear characteristic theory; ——, nonlinear characteristic theory. Characteristic network in inset.

latter three papers the authors appear to be analysing the flow system without consideration of the fluid and particulate momentum equations, a procedure whose results are questionable.

Pigford & Baron (1965) predicted, on qualitative grounds, the mechanism of shock formation in gas-particulate fluidized beds. They noted that 'A (particulate voidage) density disturbance that is initially symmetrical is distorted as it grows and moves upward, the wave crests of greater solids concentration overtaking the troughs of lower concentration above. The linear theory is not capable of following these changes, which correspond to finite amplitudes, but it is reasonable to suppose that the actual disturbances will develop in the direction indicated. The result is the development of short shock-wave structures...' This effect, postulated by Pigford & Baron, is confirmed in this paper and is shown in figure 1.

In our procedure we have solved the two-phase nonlinear conservation equations of mass and momentum by the method of characteristics and have demonstrated that a shock wave can form in the medium. Calculations have then been performed to determine the effect of the several flow parameters on shock formation. For example, calculations show that decreasing the particulate size delays shock formation, a result consistent with experimental data on bubble formation in gas-particulate fluidized beds. This same correspondence between shock formation and bubble formation is shown herein for the other parameters of the flow. It is concluded, therefore, that the shock front and the bubble front are one and the same thing.

Our procedure is analogous to that used in gas dynamics to demonstrate the formation of a shock wave in a one-phase fluid medium (as discussed, for example, by Liepmann & Roshko 1957). In gas dynamics the unsteady, one-dimensional, compressible equations for mass and momentum under the added constraint of isentropy are investigated. When the method of characteristics is applied to these nonlinear

equations, the characteristic curves have slopes which can change with time, indicating the formation of a shock wave. However, when the flow equations are linearized, the characteristic curves have constant slopes so that shock formation is impossible. The same behaviour is exhibited in our two-phase analysis.

In the two-phase system the analysis starts with the unsteady, one-dimensional, incompressible equations for mass and momentum for the fluid phase and the particulate phase, with the fluid stress tensor and particulate stress tensor neglected. Using relations for the interaction force and particulate pressure proposed by Garg & Pritchett (1975), the fluid pressure and particulate pressure are eliminated by combining the fluid momentum and the particulate momentum equations. Then, in the two-phase system there are three equations: fluid continuity, particulate continuity, and combined momentum for the three dependent variables: fluid voidage, fluid velocity, and particulate velocity. Application of the method of characteristics to these nonlinear equations gives characteristic curves which can cross, indicating the formation of a shock. On the other hand, linearization of the flow equations gives characteristic curves with constant slopes so that shock formation is impossible.

The existence of characteristics implies that the three equations, fluid continuity, particulate continuity and combined momentum, are hyperbolic. Mathematically, hyperbolicity means that there exist real characteristic curves, as many in number as there are equations, along which the partial differential equations reduce to ordinary differential equations (the compatibility relations) containing gradients along the characteristics only.

The formal application of the method of characteristics to our three equations gives only two real characteristic directions. The third compatibility relation must, therefore have an infinite slope. (A similar situation was encountered by Bradshaw, Ferriss & Atwell 1967.) Its compatibility relation is obtained from a combination of the fluid continuity and particulate continuity equations which expresses conservation of mass for the mixture and is constant for all times.

The solution of the characteristic network requires input data for the dependent variables at an initial time. For this purpose a sine function disturbance is imposed on the particulate voidage at minimum fluidization. Consistent initial conditions are determined for the other dependent variables, namely the fluid velocity and the particulate velocity.

2. Theory

A fluidized bed, under normal operating conditions, contains a two-phase high-temperature chemically reacting mixture of multispecies fluid particles and multispecies solid particles. The equations describing this phenomenon have been derived by Ness & Fanucci (1977).

In the present instance a highly specialized form of these equations is employed. A cold flow is postulated and the two-phase flow equations are investigated under the following assumptions: one fluid species $(\,)_f$, one particulate species $(\,)_p$, no chemical reactions, constant temperature, constant fluid density ($\rho_f = \text{const.}$), constant particulate density ($\rho_p = \text{const.}$), zero fluid shear stress ($\tilde{\tau}_f = 0$), zero particulate shear stress ($\tilde{\tau}_p = 0$). Under these assumptions, the fluid and particulate energy equations are not

required and the continuity and momentum equations for the fluid phase become, respectively,

$$\frac{\partial \epsilon_f}{\partial t} + \nabla . \epsilon_f \mathbf{v}_f = 0, \tag{1}$$

$$\epsilon_f \rho_f \frac{\partial \mathbf{v}_f}{\partial t} + \epsilon_f \rho_f (\mathbf{v}_f . \nabla) \mathbf{v}_f + \nabla \epsilon_f p_f - \epsilon_f \rho_f \mathbf{g} + \epsilon_p \rho_p \mathbf{f}_p = 0, \tag{2}$$

while for the particulate phase they become:

$$\frac{\partial \epsilon_p}{\partial t} + \nabla . \epsilon_p \mathbf{v}_p = 0, \tag{3}$$

$$\epsilon_p \rho_p \frac{\partial \mathbf{v}_p}{\partial t} + \epsilon_p \rho_p (\mathbf{v}_p . \nabla) \mathbf{v}_p + \nabla \epsilon_p p_p - \epsilon_p \rho_p \mathbf{g} - \epsilon_p \rho_p \mathbf{f}_p = 0. \tag{4}$$

Equations for cold flow for a single fluid species and a single particulate species have been previously advanced by Murray (1965) and Anderson & Jackson (1967).

In these equations, ϵ_f and ϵ_p are the fluid and particulate voidages, respectively, related by $\epsilon_f + \epsilon_p = 1$; also $\mathbf{v}_f$, $\mathbf{v}_p$ are the fluid and particulate velocities, respectively; p_f, p_p are the fluid and particulate static pressures, respectively; $\mathbf{g}$ is the acceleration vector while the grouping $\epsilon_p \rho_p \mathbf{f}_p$ is the interaction force per unit volume.

The relations proposed by Garg & Pritchett (1975) for the interaction force and the particulate pressure are employed: $\epsilon_p \rho_p \mathbf{f}_p = B(\epsilon_f)(\mathbf{v}_f - \mathbf{v}_p) - p_f \nabla \epsilon_f$ and $p_p = p_f + f(\epsilon_f)$ where $B(\epsilon_f)$ is the local mean drag function.

Equations (1) to (4) are specialized to one dimension and time, with the positive x co-ordinate acting opposite in direction to the gravitational acceleration vector so that $\mathbf{g} = -\hat{\mathbf{x}} g$; $\hat{\mathbf{x}}$ is a unit vector. The uniform fluidization analysis enables the gravitational acceleration to be expressed by

$$g = \frac{B_0(\epsilon_{f_0}) u_{f_0}}{(\rho_p - \rho_f) \epsilon_{f_0} \epsilon_{p_0}}, \tag{5}$$

where the subscript $(_0)$ refers to the state of uniform fluidization and u_{f_0} is the uniform fluidization velocity. Defining a particulate pressure function $G(\epsilon_f)$ and a reaction function R by:

$$G(\epsilon_f) = \frac{d}{d\epsilon_f} [\epsilon_p f(\epsilon_f)], \tag{6}$$

$$R = \frac{B_0(\epsilon_{f_0}) u_{f_0}}{\epsilon_{f_0} \epsilon_{p_0}} - \frac{B(\epsilon_f)(u_f - u_p)}{\epsilon_f \epsilon_p}, \tag{7}$$

the momentum equations (2) and (4) can be combined by eliminating the fluid pressure. Introducing the dimensionless quantities

$$x^* = \frac{x}{\lambda}, \quad t^* = \frac{u_{f_0} t}{\lambda}, \quad u_f^* = \frac{u_f}{u_{f_0}}, \quad u_p^* = \frac{u_p}{u_{f_0}},$$

$$\rho_f^* = \frac{\rho_f}{\rho_{m_0}}, \quad \rho_p^* = \frac{\rho_p}{\rho_{m_0}}, \quad G^*(\epsilon_f) = \frac{G(\epsilon_f)}{\rho_{m_0} u_{f_0}^2}, \quad R^* = \frac{\lambda R}{\rho_{m_0} u_{f_0}^2},$$

the three-equations describing the two-phase system are:

$$\frac{\partial \epsilon_f}{\partial t^*} + u_f^* \frac{\partial \epsilon_f}{\partial x^*} + \epsilon_f \frac{\partial u_f^*}{\partial x^*} = 0, \tag{8}$$

$$\frac{\partial \epsilon_f}{\partial t^*} + u_p^* \frac{\partial \epsilon_f}{\partial x^*} - \epsilon_p \frac{\partial u_p^*}{\partial x^*} = 0, \tag{9}$$

$$\rho_f^* \frac{\partial u_f^*}{\partial t^*} + \rho_f^* u_f^* \frac{\partial u_f^*}{\partial x^*} - \rho_p^* \frac{\partial u_p^*}{\partial t^*} - \rho_p^* u_p^* \frac{\partial u_p^*}{\partial x^*} - \frac{G^*(\epsilon_f)}{\epsilon_p} \frac{\partial \epsilon_f}{\partial x^*} = R^*. \tag{10}$$

λ is the wavelength of the disturbance to be imposed, u_f and u_p are, respectively, the x wise fluid and particulate velocity components, and ρ_{m_0} is defined by (17) with a subscript $(_0)$ on the voidages.

The first equation represents fluid continuity, the second equation particulate continuity, and the third equation combined momentum. These equations are hyperbolic and a solution is sought for the three dependent variables u_f^*, u_p^*, ϵ_f along characteristic lines in the x^*, t^* plane whereon the partial differential equations reduce to ordinary differential equations. Hyperbolicity of the three equations (8) to (10) means that there are an equal number (three) of real characteristic directions each with its own compatibility relation. The formal application of the method of characteristics gives only two real characteristic directions. The third characteristic therefore must have an infinite slope. (A similar situation was encountered by Bradshaw *et al.* 1967.) The slopes for the three characteristic directions are

$$\left(\frac{dx^*}{dt^*}\right)_{C_\parallel} = \infty, \tag{11}$$

$$\left(\frac{dx^*}{dt^*}\right)_{C_\pm} = V^* \pm c^*, \tag{12}$$

where $V^* = V/u_{f_0}$ and $c^* = c/u_{f_0}$; V and c are, respectively, the weighted mean velocity and the dynamic wave velocity defined by:

$$V = \frac{\dfrac{\rho_f u_f}{\epsilon_f} + \dfrac{\rho_p u_p}{\epsilon_p}}{\dfrac{\rho_f}{\epsilon_f} + \dfrac{\rho_p}{\epsilon_p}}, \tag{13}$$

$$c = \left[\frac{1}{\rho_f/\epsilon_f + \rho_p/\epsilon_p}\left\{\frac{-(u_f - u_p)^2}{\epsilon_f/\rho_f + \epsilon_p/\rho_p} - \frac{G(\epsilon_f)}{\epsilon_p}\right\}\right]^{\frac{1}{2}}. \tag{14}$$

The characteristic network is shown in the inset on the upper left-hand portion of figure 1. The curve $C_\parallel$ is a characteristic parallel to the x^* axis; the curve C_+ is a right-running characteristic obtained by taking the $(+)$ sign in (12) while the curve C_- is a left-running characteristic resulting from the $(-)$ sign in (12). Wallis (1969) obtained relations (12) to (14) by another procedure.

The compatibility relation along the parallel characteristic line $C_\parallel$ results by eliminating the time-dependent terms from (8) and (9) to provide $(\partial/\partial x^*)(\epsilon_f u_f^* + \epsilon_p u_p^*) = 0$. Integration provides $\epsilon_f u_f^* + \epsilon_p u_p^* = K(t^*)$ where $K(t^*)$ is, at most, a function only of t^*. Conservation of mass, however, dictates that $K(t^*)$ remains constant at its initial value, i.e. $K(t^*)|_{t^*=0} = \epsilon_{f_0}$. Therefore the compatibility relation along $C_\parallel$ is:

$$\epsilon_f u_f^* + \epsilon_p u_p^* = \epsilon_{f_0}. \tag{15}$$

The compatibility relations along $C_\pm$ result from the formal application of the method of characteristics to equations (8) to (10); they are

$$\rho_m^* c^* \left(\frac{d\epsilon_f}{dt^*}\right)_{C_\pm} \pm \left(\frac{dH^*}{dt^*}\right)_{C_\pm} \mp R^* = 0, \tag{16}$$

where $\rho_m^* = \rho_m/\rho_{m_0}$ and $H^* = H/\rho_{m_0} u_{f_0}$; ρ_m and H are, respectively, a weighted mean density and a mass flux difference defined by:

$$\rho_m = \frac{\rho_f}{\epsilon_f} + \frac{\rho_p}{\epsilon_p}, \tag{17}$$

$$H = \rho_f u_f - \rho_p u_p. \tag{18}$$

Equations (15) and (18) show that u_f^* and u_p^* are functions only of ϵ_f and H^* through the relations

$$u_f^* = \frac{1}{\rho_m^*}\left(\frac{\epsilon_{f_0}}{\epsilon_f \epsilon_p}\rho_p^* + \frac{H^*}{\epsilon_f}\right), \tag{19}$$

$$u_p^* = \frac{1}{\rho_m^*}\left(\frac{\epsilon_{f_0}}{\epsilon_f \epsilon_p}\rho_f^* - \frac{H^*}{\epsilon_p}\right). \tag{20}$$

Thus the quantities V^*, c^*, R^* which appear in the slope equations and/or the compatibility relations along the $C_\pm$ characteristic lines are functions only of ϵ_f and H^*.

The total derivatives in the compatibility relations (16) apply only along the characteristic lines $C_\pm$. However, since

$$\left(\frac{d}{dt^*}\right)_{C_\pm} = \frac{\partial}{\partial t^*} + (V^* \pm c^*)\frac{\partial}{\partial x^*}, \tag{21}$$

equation (16) becomes

$$\rho_m^* c^* \left[\frac{\partial \epsilon_f}{\partial t^*} + (V^* \pm c^*)\frac{\partial \epsilon_f}{\partial x^*}\right] \pm \left[\frac{\partial H^*}{\partial t^*} + (V^* \pm c^*)\frac{\partial H^*}{\partial x^*}\right] \mp R^* = 0. \tag{22}$$

Adding these two relations provides

$$\rho_m^* \frac{\partial \epsilon_f}{\partial t^*} + \rho_m^* V^* \frac{\partial \epsilon_f}{\partial x^*} + \frac{\partial H^*}{\partial x^*} = 0, \tag{23}$$

while subtracting the same two relations gives

$$\frac{\partial H^*}{\partial t^*} + V^* \frac{\partial H^*}{\partial x^*} + \rho_m^* c^{*2} \frac{\partial \epsilon_f}{\partial x^*} - R^* = 0. \tag{24}$$

Equations (23) and (24) are not restricted to the $C_\pm$ characteristic lines. They are used in the next section to determine the starting condition for the H^* function. Equations (23) and (24) can also be obtained directly from the original flow equations (8) to (10).

3. Method of solution

At $t^* = 0$ a sine wave disturbance is imposed on the uniform particulate voidage. It is assumed that

$$\epsilon_p = \epsilon_{p_0} + A \sin 2\pi x^*, \tag{25}$$

where A is the amplitude of the disturbance. Consistent with this assumption, the initial distribution of the H^* function is required. For this purpose (23) and (24) are used. Since the form for ϵ_p at $t^* = 0$ is assumed it follows that, at $t^* = 0$, $H^* = H^*(\epsilon_f)$ only. Thus

$$\frac{\partial H^*}{\partial t^*} = \frac{dH^*}{d\epsilon_f}\frac{\partial \epsilon_f}{\partial t^*} \quad \text{and} \quad \frac{\partial H^*}{\partial x^*} = \frac{dH^*}{d\epsilon_f}\frac{\partial \epsilon_f}{\partial x^*}. \tag{26}$$

Equation (23) provides

$$\frac{\partial \epsilon_f}{\partial t^*} + V^*\frac{\partial \epsilon_f}{\partial x^*} = -\frac{1}{\rho_m^*}\frac{dH^*}{d\epsilon_f}\frac{\partial \epsilon_f}{\partial x^*}, \tag{27}$$

while (24) becomes

$$\frac{\partial \epsilon_f}{\partial t^*} + V^*\frac{\partial \epsilon_f}{\partial x^*} = \frac{1}{dH^*/d\epsilon_f}\left[-\rho_m^* c^{*2}\frac{\partial \epsilon_f}{\partial x^*} + R^*\right]. \tag{28}$$

Equating (27) and (28) and noting that $\epsilon_f = \epsilon_f(x^*)$ only at $t^* = 0$ gives

$$\frac{dH^*}{dx^*} = \pm\left[\left(\rho_m^* c^*\frac{d\epsilon_f}{dx^*}\right)^2 - \rho_m^* R^*\frac{d\epsilon_f}{dx^*}\right]^{\frac{1}{2}}, \tag{29}$$

with the starting condition $H^*(x^* = 0) = \rho_f^*$. Equation (29) is solved by the Runge–Kutta method. However, calculations showed that (29) did not produce a periodic distribution of the H^* function. That is, just as $\epsilon_p(x^* = 0) = \epsilon_p(x^* = 1)$ from (25) it is also required that the H^* function be periodic, i.e. $H^*(x^* = 0) = H^*(x^* = 1)$. This latter condition is satisfied only if $R^* \equiv 0$ at $t^* = 0$. Then the differential equation for the H^* function at $t^* = 0$ becomes

$$\frac{dH^*}{dx^*} = \pm\rho_m^* c^*\frac{d\epsilon_f}{dx^*}, \tag{30}$$

with the starting condition $H^*\ (x^* = 0) = \rho_f^*$.

The characteristic network is solved by assuming that all conditions at points 1 and 2 are known (inset of figure 1) and by applying the finite difference technique to the derivatives. Then the slope equations (12) give for the co-ordinates at point 3:

$$t_3^* = \frac{x_2^* - x_1^* + (V^* + c^*)_1 t_1^* - (V^* - c^*)_2 t_2^*}{(V^* + c^*)_1 - (V^* - c^*)_2}, \tag{31}$$

$$x_3^* = x_2^* + (V^* - c^*)_2 (t_3^* - t_2^*), \tag{32}$$

and the compatibility equations (16) give for the fluid voidage and H^* at point 3:

$$\epsilon_{f_3} = \frac{1}{\rho_{m_1}^* c_1^* + \rho_{m_2}^* c_2^*}\left[\rho_{m_1}^* c_1^*\epsilon_{f_1} + \rho_{m_2}^* c_2^*\epsilon_{f_2} + H_1^* - H_2^* + R_1^*(t_3^* - t_1^*) - R_2^*(t_3^* - t_2^*)\right], \tag{33}$$

$$H_3^* = H_2^* + \rho_{m_2}^* c_2^*(\epsilon_{f_3} - \epsilon_{f_2}) + R_2^*(t_3^* - t_2^*). \tag{34}$$

In the present case, at the start of the analysis, points 1 and 2 lie on the x^* axis with $t_1^* = t_2^* = 0$. Then, for chosen values of x_1^* and x_2^*, ϵ_{p_1} and ϵ_{p_2} follow from (25); integration of (30) gives the corresponding H_1^* and H_2^* while (19) and (20) give $u_{f_3}^*$ and $u_{p_3}^*$. In the actual solution of the characteristic network an iterative procedure is used to find conditions at point 3.

Figure	A	$\lambda(m)$	$G(\epsilon_f)$ (N/m³)	$r \times 10^4$ (m)	ϵ_{f_0}	u_{f_0} (m/s)	$\mu_f \times 10^5$ (kg m^{-1} s^{-1})	ρ_p (kg/m³)	ρ_f (kg/m³)
1	0·03	0·0086	−1800	4·3	0·5	1·323	1·827	3000	1·2
2	0·03	0·0086	−1800	4·3	0·5	1·323	1·827	3000	1·2
3	0·01	0·0086	Variable	1·6	0·4	0·09971	1·827	3000	1·2
4	0·01	0·0086	Variable	1·6	0·4	0·09971	1·827	3000	1·2
5	0·01	0·0086	−1800	Variable	0·4	*	1·827	3000	1·2
6	0·01	0·0086	−1800	4·3	Variable	*	1·827	3000	1·2
7	0·01	0·0086	−1800	4·3	0·4	*	Variable	3000	1·2
8	0·01	0·0086	−1800	4·3	0·4	*	1·827	Variable	1·2

* Related to 'Variable' parameter through equation (5).

TABLE 1. Parameters for figures 1 to 8.

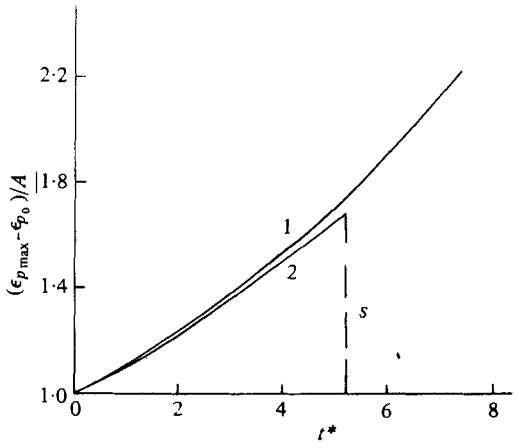

FIGURE 2. Growth of the maximum particulate voidage with time. Curve 1, linear stability theory of Garg & Pritchett (1975); curve 2, nonlinear theory; s, shock forms.

The expression used for the local mean drag function $B(\epsilon_f)$ is that suggested by Garg & Pritchett (1975):

$$B(\epsilon_f) = \frac{9}{2}\frac{\epsilon_f \epsilon_p}{r^2}\mu_f \exp\left[(4{\cdot}093 - 0{\cdot}3625\epsilon_f)\left(\frac{\epsilon_p}{\epsilon_f}\right)^{\frac{1}{3}}\right], \tag{35}$$

where r is the particulate radius and μ_f is the fluid dynamic viscosity.

4. Results and conclusions

There are nine parameters in the analysis: A, amplitude of the initial disturbance; λ, wavelength of the initial disturbance; $G(\epsilon_f)$ particulate pressure function; r, particulate radius; ϵ_{f_0}, uniform fluidization voidage; u_{f_0}, fluidization velocity; μ_f, fluid dynamic viscosity; ρ_p, particulate density; ρ_f, fluid density. The parameters A, λ, $G(\epsilon_f)$ are independent of each other and of the other six. The remaining six parameters are related through (5). Table 1 contains the values of the parameters for figures 1 to 8. The values for $r(= 4{\cdot}3 \times 10^{-4}$ m), μ_f $(= 1{\cdot}827 \times 10^{-5}$ kg/m$-$s), ρ_p $(= 3000$ kg/m^3), ρ_f $(= 1{\cdot}2$ kg/m^3) are those used by Garg & Pritchett (1975). A and ϵ_{f_0} are already dimensionless; the other seven parameters provide the four dimensionless groups: $\lambda/r, \rho_p/\rho_f, G(\epsilon_f)/\rho_p u_{f_0}^2, \rho_f u_{f_0} r/\mu_f$. Values for these dimensionless groups can be readily calculated from the numbers given in table 1.

All calculations in this report are based on the whole-field perturbation assumption, i.e. the uniformly fluidized bed is perturbed by an infinite number of contiguous sine waves for ϵ_p [equation (25)] starting at $x^* = 0$. The stability of the uniformly fluidized bed is reflected in the time and distance for shock formation, that is, the greater the time and distance for shock formation the more stable is the fluidized bed.

Figure 1 shows the propagation of the particulate voidage ϵ_p with time and distance. The results of two different theories are presented. In one, the flow equations are linearized and the method of characteristics is employed for a solution. This procedure is identical to the nonlinear analysis except that, for the linear analysis, the characteristic lines have constant slope and a particulate voidage of increasing amplitude with time and distance (dashed curves). These dashed curves retain their original 'sinu-

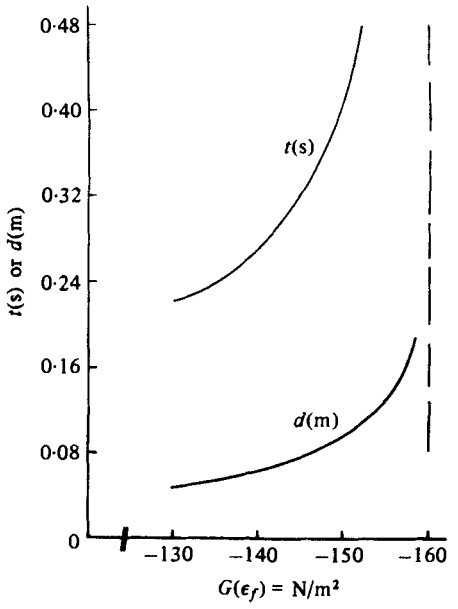

FIGURE 3. Effect of particulate pressure function $G(\epsilon_f)$ on shock formation. $t(s)$, time for shock formation; $d(m)$, distance for shock formation.

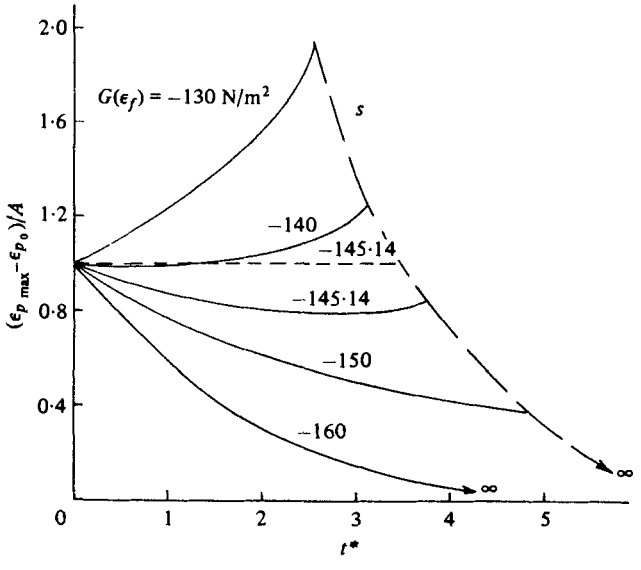

FIGURE 4. Maximum particulate voidage as a function of t^* and $G(\epsilon_f)$. ----, $G(\epsilon_f) = -145{\cdot}14$ N/m² is the value for neutral stability according to Garg & Pritchett (1975). s, shock forms.

soidal' shape with time and distance and cannot roll up into a discontinuity because of the constancy of their characteristic slopes. In the second theory the method of characteristics is applied to the nonlinear equations as discussed in this paper. Now the characteristic lines cross (as shown in the figure) and the original sinusoidal shape for ϵ_p rolls up into a discontinuity at the crossing point. This effect was predicted, on

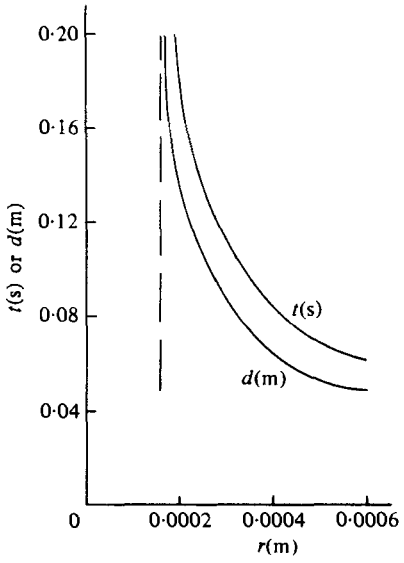

FIGURE 5. Effect of particulate radius r on time and distance for shock formation.

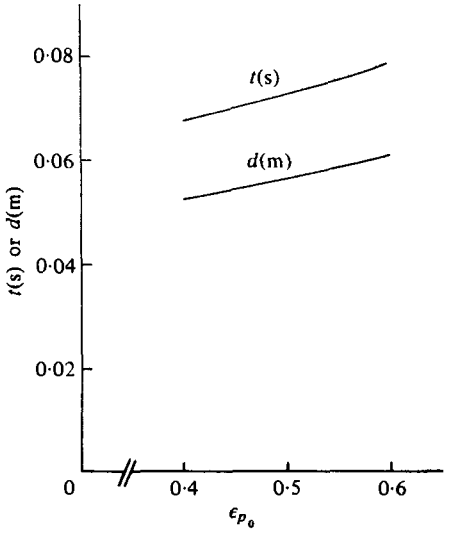

FIGURE 6. Effect of uniform particulate voidage ϵ_{p_0} on time and distance for shock formation.

qualitative grounds, by Pigford & Baron (1965). The time to the crossing point is $t = 0{\cdot}0338$ s and the distance $d = (3{\cdot}6\text{–}0{\cdot}5)\,\lambda = 0{\cdot}02666$ m. Also shown on the figure is the scale for ϵ_p.

Figure 2 shows the growth of the maximum particulate voidage with time according to the linear stability theory of Garg & Pritchett (1975) (curve 1) and the present nonlinear analysis (curve 2). The linear stability curve follows from the relation

$$\frac{\epsilon_{p_{\max}} - \epsilon_{p_0}}{A} = \exp \xi t \tag{36}$$

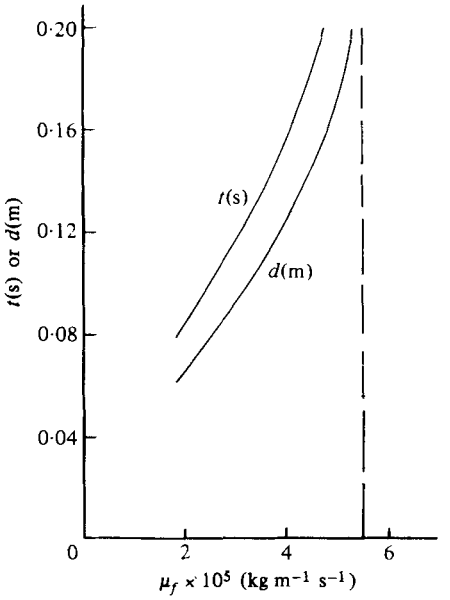

FIGURE 7. Effect of fluid viscosity μ_f on time and distance for shock formation.

where, for the parameters of figure 2, $\xi = 16{\cdot}53$ s^{-1}. According to linear stability theory, instability occurs when $\xi > 0$. In the present case, the Garg & Pritchett curve increases, without end, for all time since there is no mechanism in the analysis for a shock to occur. The nonlinear analysis, however, indicates that a shock forms at $t = 0{\cdot}0338$ s, at which time the nonlinear analysis ends. There is, however, a close correlation between linear and nonlinear theory for the range of applicability of the latter analysis.

Figure 3 shows the effect of the particulate pressure function on the time t (in seconds) and the distance d (in metres) for shock formation. The $G(\epsilon_f)$ function acts like a compressibility factor with an increase (negatively) in $G(\epsilon_f)$ producing an increase in the dynamic wave velocity c (14). In the limit as $G(\epsilon_f) \to -\infty$, $c \to \infty$, i.e. the bed behaves as an incompressible fluid in gas dynamics. Figure 3 shows, correctly, that as the bed becomes more 'incompressible' (that is, as $G(\epsilon_f)$ increases negatively) there is less chance for a shock to occur.

Figure 4 shows the maximum particulate voidage as a function of time and the particulate pressure function $G(\epsilon_f)$ for the same parameters as in figure 3. The solid curves for the indicated values of $G(\epsilon_f)$ result from the nonlinear theory. The dashed curve for $G(\epsilon_f) = -145{\cdot}14$ N/m^2 is for neutral stability according to Garg & Pritchett (1975) and is obtained from equation (47) of their paper. The dashed curve indicating shock formation is a replot (in dimensionless time) of the time curve of figure 3. For $G(\epsilon_f) = -130$ N/m^2, the maximum particulate voidage increases with time and the calculations end when the shock forms. However, as $G(\epsilon_f)$ increases negatively, the calculations show that $\epsilon_{p_{\max}}$ can decrease below its original maximum ($= 0{\cdot}61$) and still produce a shock. This result is contrary to linear stability theory in that it shows that a negative growth rate does not necessarily imply stability. When $G(\epsilon_f) = -160$ N/m^2 the perturbations damp out, indicating stability.

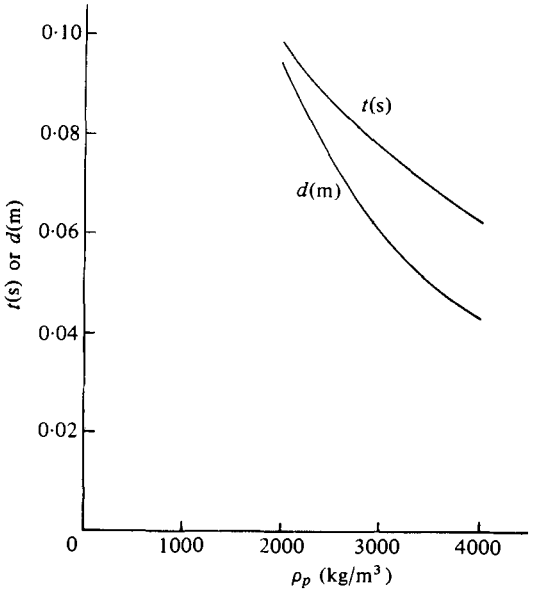

FIGURE 8. Effect of particulate density ρ_p on time and distance for shock formation.

Figure 5 shows the effect of the particulate radius r on the time and distance for shock formation. The curves indicate that decreasing the particulate radius increases the bed stability. This result is in agreement with experimental data as stated by El-Kaissy & Homsy (1976): '... beds of very fine particles will not bubble until conditions removed from minimum fluidizations are reached'.

Figure 6 shows the effect of the uniform particulate voidage ϵ_{p_0} on the time and distance for shock formation. It is noted that as ϵ_{p_0} increases, that is, the bed becomes more dense, it becomes more stable, a result in agreement with the Garg & Pritchett (1975) statement: '... dense fluidized beds are more stable than dilute fluidized beds'.

Figure 7 shows the effect of the fluid viscosity μ_f on the time and distance for shock formation. The results indicate that increasing μ_f increases the bed stability.

Figure 8 shows the effect of the particulate density ρ_p on the time and distance for shock formation. The curves indicate that increasing ρ_p (or ρ_p/ρ_f since ρ_f is constant) decreases stability and increases the possibility of bubbling. This result is in agreement with the statement by Rowe (1971): 'The most important parameter in determining bubbling is the ratio of solid to fluid density and if this exceeds about 10, the system is likely to bubble.'

The calculations in this paper are based on a local mean drag function $B(\epsilon_f)$ suggested by Garg & Pritchett (1975) and which, according to them, is 'strictly speaking, only valid for water-fluidized glass spheres.' In addition, calculations herein are based on assumed constant values for the particulate pressure function $G(\epsilon_f)$. It is hoped that more realistic expressions for these functions, when they become available, will not alter the qualitative results herein.

In conclusion, it has been demonstrated by the method of characteristics that a small disturbance imposed on the nonlinear two-phase flow equations can, with time, produce a discontinuity similar to a shock wave in gases. A study of the parameters entering the problem indicates that the following factors delay shock formation: a

decrease in particulate size, an increase in bed density, an increase in fluid viscosity, and a decrease in particulate density. Experimental data on bubble formation in gas-particulate fluidized beds show that these same factors delay bubble formation. It is hypothesized, therefore, that the shock front and the bubble front are one and the same thing.

If this hypothesis is correct, that the origin of the bubble is due to the formation of a shock wave, then it follows that the initial velocity of a single rising bubble is equal to the shock wave velocity at the instant of shock formation. To predict bubble velocity, many authors currently employ the Davies & Taylor (1950) expression for the rising velocity of a bubble formed from trapped air, initially at rest, in a stationary column of liquid. This relation is $u_b = 0{\cdot}711(gD_e)^{\frac{1}{2}}$ and relates the bubble velocity u_b (m/s) to the equivalent bubble diameter $D_e(m)$; it implies that $u_b \to 0$ as $D_e \to 0$. However, its extension to the formation of bubbles in a fluidized bed is questionable. In fact, inspection of the test data in Calderbank, Pereira & Burgess (1976) relating u_b to D_e indicates that a finite velocity in the limit when $D_e \to 0$ is highly feasible. The shock wave velocity at the instant of shock formation must be determined from the jump relations across a moving shock wave in a gas-particulate fluidized bed. The authors of this paper are currently engaged in this task.

Details of the analysis in this paper, the computer program, and additional results are contained in a report by Fanucci, Ness & Yen (1978).

This research was started under USERDA Morgantown Energy Research Center Contract EY-77-C-21-8087, Task Order No. 8, and completed under funding from the state of West Virginia to West Virginia University for energy research.

REFERENCES

ANDERSON, T. B. & JACKSON, R. 1967 A fluid mechanical description of fluidized beds. *Ind. Eng. Chem. Fundamentals*, **6**, 527–539.

BRADSHAW, P., FERRISS, D. H. & ATWELL, N. P. 1967 Calculation of boundary-layer development using the turbulent energy equation. *J. Fluid Mech.* **28**, 596.

CALDERBANK, P. H., PEREIRA, J. & BURGESS, J. M. 1976 The physical and mass transfer properties of bubbles in fluidized beds of electrically conducting particles. In *Fluidization Technology*, vol. 1 (ed. D. L. Keairns), p. 158. Washington: Hemisphere Publishing Corporation.

DAVIES, R. M. & TAYLOR, G. I. 1950 The mechanics of large bubbles rising through extended liquids and through liquids in tubes. *Proc. Roy. Soc.* A, **200**, 375–390.

EL-KAISSY, M. M. & HOMSY, G. M. 1976 Instability waves and the origin of bubbles in fluidized beds. *Int. J. Multiphase Flow* **2**, 379–395.

FANUCCI, J. B., NESS, N. & YEN, R.-H. 1978 On the formation of bubbles in gas-particulate fluidized beds. Department of Aerospace Engineering, West Virginia University, Morgantown, West Virginia, TR-62.

GARG, S. K. & PRITCHETT, J. W. 1975 Dynamics of gas-fluidized beds. *J. Appl. Phys.* **46**, 4493–4500.

JACKSON, R. 1963 Part I The mechanics of fluidised beds. Part I: The stability of the state of uniform fluidisation. *Trans. Instn Chem. Engrs.* **41**, 13–21.

JACKSON, R. 1963 Part II. The mechanics of fluidised beds; Part II. The motion of fully developed bubbles. *Trans. Instn Chem. Engrs.* **41**, 22–28.

LIEPMAN, H. W. & ROSHKO, A. 1957 *Elements of Gasdynamics*, p. 76. Wiley.

MURRAY, J. D. 1965 On the mathematics of fluidization. Part 1. Fundamental equations and wave propagation. *J. Fluid Mech.* **21**, 465–493.

NESS, N. & FANUCCI, J. B. 1977 Fluidized bed flow equations. Department of Aerospace Engineering, West Virginia University, Morgantown, West Virginia, TR-56.

PIGFORD, R. L. & BARON, T. 1965 Hydrodynamic stability of a fluidized bed. *Ind. Eng. Chem. Fundamentals*, **4**, 81–87.

ROWE, P. N. 1971 Experimental properties of bubbles. In *Fluidization* (eds. J. F. Davidson & D. Harrison) p. 186. Academic Press.

RUCKENSTEIN, E. & TZECULESCU-FILIPESCU, M. 1967 On the hydrodynamics of the fluidized bed. *Proc. Inter. Symp. Fluidization*, p. 180. Netherlands Univ. Press-Amsterdam.

VERLOOP, J. & HEERTJES, P. M. 1970 Shock waves as a criterion for the transition from homogeneous to heterogeneous fluidization. *Chem. Engng Sci.* **25**, 825–832.

VERLOOP, J. & HEERTJES, P. M. 1974 On the origin of bubbles in gas-fluidized beds. *Chem. Engng. Sci.* **29**, 1101–1107.

VERLOOP, J., HEERTJES, P. M. & LERK, L. A. 1974 The velocity and stability of large porosity fluctuations in homogeneous fluidized systems. *Chem. Engng Sci.* **29**, 1109–1114.

WALLIS, G. B. 1962 A simplified one-dimensional representation of two-component vertical flow and its application to batch sedimentation. *Symp. Interact. Fluids and Particles*, pp. 9–16.

WALLIS, G. B. 1969 *One-dimensional two-phase flow*, p. 139. McGraw-Hill.